double bond character being granted to a formal single bond by mixing through delocalization of a radical's unpaired electron with a molecule's π bond one C atom away. It is seen for radicals which can be described in VBT hybridization terms as asymmetric sp^2 hybrids on C. It is absent from symmetrical sp^2's, from sp^3's, and sp hybrid structures. Acrylamide, methyl acrylate, ethyl methacrylate, and acrylic acid show the effect, whereas acrylonitrile, styrene, allylbenzene, and uracil do not. Since muonium reacts with these molecules on its first encounter, it implies that the cis-trans distribution found in the radical represents that present in the parent molecule.

Acknowledgment. We greatly appreciate the collaboration of John M. Stadlbauer, Zhennan Wu, and Alicia Gonzalez in these studies and the continued help from Curtis Ballard and Keith Hoyle. NSERC of Canada provided some of the funds needed.

Theoretical Study of Pseudorotation of Pentacoordinated Silicon Anions: The Prototypical SiH_5^-

Mark S. Gordon,*,† Theresa L. Windus,† Larry W. Burggraf,‡ and Larry P. Davis‡

Contribution from the Department of Chemistry, North Dakota State University, Fargo, North Dakota 58105, and Directorate of Chemical and Atmospheric Sciences, Air Force Office of Scientific Research, Bolling AFB, Washington, D.C. 20332. *Received August 29, 1989*

Abstract: Ab initio and semiempirical calculations are used to analyze the minimum energy path for the pseudorotation of SiH_5^-. Both AM1 and MP2/6-31++G(d,p) predict pseudorotation barriers of 2.4 kcal/mol. A decomposition of the projected vibrational frequencies along the path is used to assist in the interpretation of the process.

Introduction

Pentacoordinated silicon compounds preferentially bond in trigonal-bipyramidal (tbp) shapes rather than square-pyramidal (spy) or other geometries.[1] In the tbp geometry, the substituents can assume either one of the two axial positions or one of the three equatorial positions. Depending on the nature of the substituents, any or all of the possible permutations of the ligands may or may not be stable structures. For example, in the model compound SiX_4Y^-, two distinguishable isomers are predicted, one with Y axial and the other with Y equatorial. With a larger variety of substituents, there are a proportionately larger number of possible isomers of the pentacoordinated structure.

These stereoisomers of simple pentacoordinated silicon compounds are not experimentally separable at room temperature; rapid ligand exchange occurs between the axial and equatorial positions.[2] There has been a large body of work devoted to understanding these processes in the analogous pentacoordinated phosphorus compounds,[3-7] and studies of pentacoordinated silicon make use of this body of work as a base. Differences between the two systems will be strongly dictated by the more electropositive nature of the silicon atom as compared with phosphorus[8] and to the presence of a formal negative charge on silicon.

One possible mode for rapid ligand exchange is the process of pseudorotation. Strauss defines pseudorotation as an intramolecular motion of nuclei in a molecule in which conformers interchange to equivalent structures differing only by the number of the atoms.[9] In a broader sense, pseudorotation can also include the exchange of nonequivalent nuclei to produce a trigonal-bipyramidal stereoisomer of the original structure. Berry proposed a specific type of pseudorotation, now widely known as Berry pseudorotation, to explain fluxional behavior of phosphoranes.[10] This Berry pseudorotation process is now widely used to explain isomerization phenomena in 10-electron systems.[11] In this mechanism, shown in Figure 1, a single equatorial substituent (the pivot group) is held stationary, while the two axial ligands become equatorial and the two equatorial ligands become axial. At some intermediate point in the process, a square-pyramidal structure is formed with the four interconverting ligands forming basal positions in the pyramid and the pivot ligand occupying an apical position in the pyramid (see Figure 1). If all ligands are equivalent, the trigonal-bipyramidal structures have D_{3h} symmetry while the square-pyramidal structure has C_{4v} symmetry. In this case, the path joining the C_{4v} and D_{3h} structures will have C_{2v} symmetry. There are a number of other types of pseudorotations that are possible: see either Musher[12] or Gillespie et al.[13] for discussion of all possible rearrangements of these systems.

The prototypical pentacoordinated silicon compound, SiH_5^-, anion has recently been observed in the gas phase.[14] A number of calculations have been done on this and related systems at both the semiempirical and ab initio levels of theory, as recently reviewed by Burggraf, Davis, and Gordon.[15] Predictions at all levels of theory confirm that the D_{3h} pentacoordinated trigonal-bipyramidal structure is a minimum on the potential surface and the C_{4v} tetragonal pyramid is higher in energy, but only a few studies have addressed the nature of the tetragonal structure as a transition state for Berry pseudorotation. Reed and Schleyer have done the most extensive characterization of the SiH_5^- system to date,

† North Dakota State University.
‡ Air Force Office of Scientific Research.

(1) Burdett, J. K. *Struct. Bonding (Berlin)* **1976**, *31*, 67.
(2) Carre, F. H.; Corriu, R. J. P.; Guerin, C.; Henner, B. J. L.; Wong Chi Man, W. W. C. *J. Organomet. Chem.* **1988**, *347*, C1-C4.
(3) Rauk, A.; Allen, L. C.; Mislow, K. *J. Am. Chem. Soc.* **1972**, *94*, 3035-3040.
(4) Musher, J. I. *Angew. Chem., Int. Ed. Engl.* **1969**, *8*, 54.
(5) Hoffman, R.; Howell, J. M.; Muetterties, E. L. *J. Am. Chem. Soc.* **1972**, *94*, 3047.
(6) Florey, J. B.; Cusachs, L. C. *J. Am. Chem. Soc.* **1972**, *94*, 3040.
(7) (a) *Pentacoordinated Phosphorus-Structure and Spectroscopy*; ACS Monograph 175; American Chemical Society: Washington, DC, 1980; Vols. I and II. (b) Deiters, J. A.; Holmes, R. R. *J. Am. Chem. Soc.* **1987**, *109*, 1686-1692, 1692-1696.
(8) Muetterties, E. L. *Acc. Chem. Res.* **1970**, *3*, 226.
(9) Strauss, H. L. *Annu. Rev. Phys. Chem.* **1983**, *34*, 301-328.
(10) Berrry, R. S. *J. Chem. Phys.* **1960**, *32*, 933-938.
(11) Mislow, K. *Acc. Chem. Res.* **1970**, *3*, 321.
(12) Musher, J. I. *J. Chem. Educ.* **1974**, *51*, 94-97.
(13) Gillespie, P.; Hoffman, P.; Klusacek, H.; Marquarding, D.; Pfohl, S.; Ramirez, F.; Tsolis, E. A.; Ugi, I. *Angew. Chem., Int. Ed. Engl.* **1971**, *10*, 687-715.
(14) Hajdasz, D. J.; Squires, R. R. *J. Am. Soc.* **1986**, *108*, 3139.
(15) Burggraf, L. W.; Davis, L. P.; Gordon, M. S. *Topics Phys. Organomet. Chem.*, **1989**, *3*, 75.

0002-7863/90/1512-7167$02.50/0

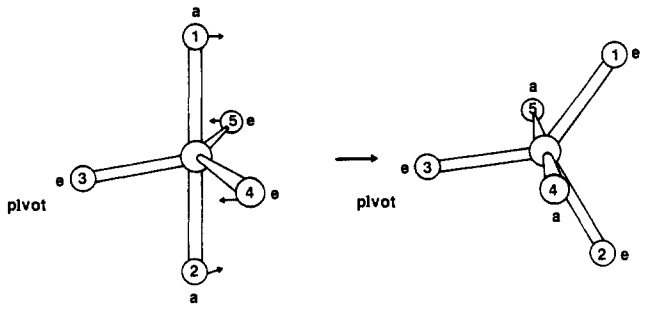

Figure 1. Illustration of Berry pseudorotation.

showing that the tetragonal structure was indeed a transition state by a force constant analysis.[16] Wilhite and Spialter modeled systems of the type $SiH_{5-n}X_n^-$ (X more electronegative than H) in order to compare the energetics of various conformers of this series with regard to Berry pseudorotation. They concluded that Berry pseudorotation was more facile when the C_{4v} tetragonal-pyramid transition state had the more electropositive substituent in the apical position.[17] Deiters and Holmes have studied the Berry pseudorotation barriers in SiH_4X^- (X = halogen) as part of a model explaining stereochemistry of nucleophilic attack on silicon compounds.[7]

Pentacoordinated species having structures which range from trigonal bipyramidal to square pyramidal along an expected generalized Berry pseudorotational pathway have been found experimentally.[18] These observations lend some experimental credence to the Berry mechanism.

The purpose of this paper is to begin a systematic study of Berry pseudorotation processes in pentacoordinated silicon compounds, including characterizations of the potential energy surfaces, force constant analyses, and intrinsic reaction coordinate (IRC) calculations.[19] In many mixed-ligand systems, there are a number of stable isomers predicted, while in others there are only a very few. Only through a thorough systematic analysis of these structures can we understand trends in the behavior of these compounds. These pseudorotation processes may play a major role in determining the stereochemistry of a variety of reactions involving silicon compounds.[7b]

We have found that the use of semiempirical techniques to explore surfaces in a preliminary fashion and to extend results to large systems, combined with ab initio calculations to establish limits of accuracy of semiempirical methods and produce quantitative results for small- to medium-sized systems, has been exceedingly fruitful in studying these hypervalent silicon systems.[20-22] In this initial paper, we lay the groundwork for this systematic study by considering in detail the Berry pseudorotation process in the prototypical SiH_5^- anion.

Computational Methods

All semiempirical calculations were performed with the MOPAC program.[23] Results were obtained for the MNDO,[24] AM1,[25] and PM3[26] Hamiltonians. In the case of MNDO, the silicon parameters were taken from a later publication by Dewar.[27]

All ab initio calculations were performed with a locally modified version of GAUSSIAN86.[28] Structures for all species were intially obtained at the restricted Hartree–Fock (RHF)/6-31G(d) level.[29] In addition, geometry optimizations were done at the second-order perturbation theory (MP2[30]) level with use of the 6-31G(d) and 6-31++G(d,p)[31] basis sets to assess the importance of correlation and diffuse functions in the basis set in predicting the geometries for these hypervalent species. Energies for all species were calculated at all levels of geometry optimization. In addition, energies were also calculated at the fourth-order perturbation theory level (MP4[32]) utilizing the 6-31++G(d,p) basis set. Zero-point vibrational energies were added to all electronic energies, making the differences more directly comparable to the semiempirical enthalpies. Mulliken population analyses were performed with RHF/6-31++G(d,p) wave functions.

All stationary points with all methods were verified by diagonalizing the Cartesian force constant matrices and demonstrating that minima and transition states had zero and one negative eigenvalue, respectively. For the ab initio calculations, these normal-mode frequencies were calculated at all levels of geometry optimization. For all ab initio structures, the normal modes were analyzed in terms of their component internal coordinate contributions with the vibrational decomposition method developed by Boatz and Gordon.[33]

Intrinsic reaction coordinate (IRC) calculations at the ab initio level were done utilizing the fourth-order Runge–Kutta (RK4) method.[34] The initial quadratic step off the saddle point with a 10^{-6} amu$^{1/2}$·bohr step in the direction indicated by the imaginary normal mode was followed by RK4 steps of 0.0001–0.005 amu$^{1/2}$·bohr. The latter were adjusted so as to maximize the efficiency of the calculations, while maintaining the symmetry of the path. IRC calculations were performed at the semiempirical levels of theory with the approximate intrinsic reaction coordinate method developed by Stewart, Davis, and Burggraf[35] as imple-

Table I

method	bond length (Å) R(ax)	bond length (Å) R(eq)	Si charge	H charge ax	H charge eq
MNDO	1.470	1.438	+1.872	−0.608	−0.552
AM1	1.524	1.496	+1.094	−0.499	−0.365
PM3	1.571	1.534	+0.276	−0.360	−0.186
RHF/6-31G(d)	1.622	1.531			
RMP2/6-31G(d)	1.619	1.542			
RMP2/6-31++G(d,p)	1.609	1.524	+0.617	−0.431	−0.252

Table II

method	bond length (Å) R(ap)	bond length (Å) R(bas)	A(ap) (deg)	Si charge	H charge ap	H charge bas
MNDO	1.421	1.459	104.1	+1.879	−0.527	−0.588
AM1	1.478	1.515	104.0	+1.108	−0.293	−0.454
PM3	1.509	1.559	104.2	+0.288	−0.075	−0.303
RHF/6-31G(d)	1.514	1.579	101.7			
RMP2/6-31G(d)	1.521	1.585	101.3			
RMP2/6-31++G-(d,p)	1.506	1.570	101.8	+0.631	−0.232	−0.350

(16) Reed, A. E.; Schleyer, P. R. *Chem. Phys. Lett.* **1987**, *133*, 553–561.
(17) Wilhite, D. L.; Spialter, L. *J. Am. Chem. Soc.* **1973**, *95*, 2100–2104.
(18) (a) Birgi, H. B. *Angew. Chem., Int. Ed. Engl.* **1975**, *14*, 460. (b) Mutterties, E. L.; Guggenberger, L. J. *J. Am. Chem. Soc.* **1974**, *96*, 1748. (c) Holmes, R. R.; Day, R. O.; Chandrasekhar, V.; Holmes, J. M. *Inorg. Chem.* **1985**, *24*, 2009. (d) Holmes, R. R.; Deiters, J. A. *J. Am. Chem. Soc.* **1977**, *99*, 3318.
(19) (a) Garrett, B. C.; Redman, M. J.; Steckler, R.; Truhlar, D. G.; Baldridge, K. K.; Bartol, D.; Schmidt, M. W.; Gordon, M. S. *J. Phys. Chem.* **1988**, *92*, 1476. (b) Reference 31 and references citied therein.
(20) Davis, L. P.; Burggraf, L. W.; Baldridge, K. K.; Gordon, M. S. *J. Am. Chem. Soc.* **1985**, *107*, 4415–4419.
(21) Gordon, M. S.; Davis, L. P.; Burggraf, L. W.; Damrauer, R. *J. Am. Chem. Soc.*, **1986**, *108*, 7889–7893.
(22) Davis, L. P.; Burggraf, L. W.; Gordon, M. S. *J. Am. Chem. Soc.* *1988*, *110*, 3056–3062.
(23) Stewart, J. J. P. *QCPE 455*.
(24) Dewar, M. J. S.; Theil, W. *J. Am. Chem. Soc.* **1977**, *99*, 4899–4907.
(25) Dewar, M. J. S.; Zoebisch, E. G.; Healy, E. F.; Stewart, J. J. P. *J. Am. Chem. Soc.* **1985**, *107*, 3902.
(26) Stewart, J. J. P. *J. Comput. Chem.*, in press.
(27) Dewar, M. J. S.; Healy, E. *Organometallics* **1982**, *1*, 1705–1708.
(28) Frisch, M. J.; Binkley, J. S.; Schlegel, H. B.; Raghavachari, K.; Melius, C. F.; Martin, R. L.; Stewart, J. J. P.; Brobrowicz, F. W.; Rohlfing, C. M.; Kahn; DeFrees, D. J.; Seeger, R.; Whiteside, R. A.; Fox, D. J.; Fluder, E. M.; Topiol, S.; Pople, J. A. *GAUSSIAN86*; Carnegie-Mellon Quantum Chemistry Publishing Unit: Pittsburgh, PA 15213, 1986.
(29) Hariharan, P. C.; Pople, J. A. *Theor. Chim. Acta* **1973**, *28*, 213–222. Francl, M. M.; Pietro, W. J.; Hehre, W. J.; Binkley, J. S.; Gordon, M. S.; DeFrees, D. J.; Popel, J. A. *J. Chem. Phys.* **1982**, *77*, 3654–3665. Gordon, M. S. *Chem Phys Lett.* **1980**, *76*, 163–168.
(30) Pople, J. A.; Binkley, J. S.; Seeger, R. *Int. J. Quantum Chem.* **1976**, *S10*, 1–19.
(31) Frisch, M. J.; Pople, J. A.; Binkley, J. S. *J. Chem. Phys.* **1984**, *80*, 3265.
(32) Krishman, R.; Frisch, M. J.; Pople, J. A. *J. Chem. Phys.* **1980**, *72*, 4244.
(33) Boatz, J. A.; Gordon, M. S. *J. Phys. Chem.* **1989**, *93*, 819.
(34) Baldridge, K. K.; Gordon, M. S.; Steckler, R.; Truhlar, D. G. *J. Phys. Chem.*, **1989**, *93*, 5107.

Table III. Energy Differences between D_{3h} and C_{4v} Structures of SiH_5^-

method	$\Delta E'$ (kcal/mol)	$\Delta H'$ [a] (kcal/mol)
MNDO		1.8
AM1		2.4
PM3		3.3
RHF/6-31G(d)	3.0	
RMP2/6-31G(d)	2.5	2.2
RMP2/6-31++G(d,p)	2.7	2.4
RMP4/6-31++G(d,p)[b]	2.5	2.2

[a] For the semiempirical methods, the enthalpy difference is calculated at 298 K. For the ab initio methods, the enthalpy difference is calculated at 0 K by making a zero-point energy correction to the energy difference. [b] Computed at the RMP2/6-31++G(d,p) geometry.

mented in MOPAC. Generalized normal-mode frequencies along the reaction path were obtained by projecting the $3N - 7$ transverse normal modes in a space orthogonal to the reaction path, in the manner prescribed by Miller, Handy, and Adams.[36]

Results and Discussion

Table I gives the complete set of optimized bond lengths for all levels of theory for the D_{3h} trigonal-bipyramidal structure of SiH_5^-. These results agree very well with previous calculations as discussed in our recent review paper.[15] Note that the semiempirical methods underestimate the Si–H bond lengths, with the recent PM3 method giving results closest to the ab initio results. There is very little change in geometry in improving the RHF/6-31G(d) optimization to include electron correlation at the MP2 level or diffuse functions in the basis set. Table II gives the analogous information for the C_{4v} tetragonal-pyramidal structure of SiH_5^-. Again, the semiempirical methods underestimate the Si–H bond lengths, and inclusion of electron correlation or diffuse basis set functions in the ab initio results makes little difference. A comparison of Tables I and II shows that all methods give the following trend in the lengths of the Si–H bonds: $R_{ax} > R_{bas} > R_{eq} > R_{ap}$. Tables I and II also give the Mulliken charges for each of the atoms for each structure according to each method. The trend in the charges on the hydrogen mimics the trends in the Si–H bonds; a higher negative charge on the hydrogen corresponds to a longer, and more ionic, Si–H bond. MNDO and AM1 tend to predict a higher positive charge on the silicon than does the ab initio calculation. This tendency has previously been ascribed primarily to the hydrogens being predicted with too large a negative charge.[22] PM3 generally predicts a lower positive charge than does the ab initio calculation.

Differences in energy (and/or enthalpy) between the two SiH_5^- structures are given in Table III. All methods agree that the Berry pseudorotation barrier for SiH_5^- is about 2.0 kcal/mol. These results also agree with previous calculations on this system.[15] For example, Reed and Schleyer obtained an energy difference of 2.17 kcal/mol at the RMP4/6-31++G(d,p) level of theory corrected for zero-point energies obtained at the HF/6-31+G(d) level.[16] It is obvious that the Berry pseudorotation barrier is quite small in this system and that even simple levels of theory can account for it properly.

Cartesian force constant calculations along with harmonic normal-mode frequencies were calculated for both structures with all semiempirical methods and several ab initio levels of theory. These results are given for the D_{3h} minimum of SiH_5^- in Table IV.

We find general agreement among the various methods in these calculated frequencies. The semiempirical methods switch the lowest A'_2 vibration with the second E′ pair, but all methods predict these sets of vibrations to be fairly close in frequency. PM3 also has the two highest frequency vibrations switched. All of the semiempirical methods tend to overestimate the five highest vibrational frequencies, which are primarily Si–H stretching motions. There seems to be little difference among the ab initio results, except for the typical overestimation of frequencies at the SCF level.[37]

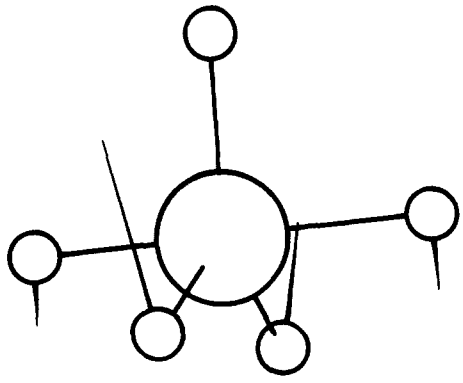

Figure 2. Illustration of normal-coordinate motion for mode ν_9, leading to pseudorotation.

An analysis of these normal-mode motions shows that the five highest frequency modes are Si–H stretches, with ν_2 and ν_3 being primarily axial stretches and ν_1, ν_5, and ν_6 being primarily equatorial stretches.

This analysis is made more quantitative in Table V, where the MP2/6-31G(d) normal modes are decomposed into their internal coordinate contributions. It is also apparent from the table that ν_4, ν_7, ν_8, ν_{11}, and ν_{12} are dominated by H_{ax}–Si–H_{eq} bending motions, whereas ν_9 and ν_{10} (as discussed in more detail below) correspond to the H_{eq}–Si–H_{eq} bend.

Mode ν_9, diagrammed in Figure 2, is one of the degenerate pair of the lowest frequency E′ symmetry vibration, and it has the motion appropriate to carrying the molecule along a Berry pseudorotation pathway. Note that the two axial hydrogens move tangentially toward each other so as to close the H_{ax}–Si–H_{ax} angle, while two of the three equatorial hydrogens (H_1 and H_2) move tangentially away from each other so as to open the H_1–Si–H_2 angle. In this motion, H_3 is the pivotal hydrogen and the other two equatorial hydrogens become axial while the two axial hydrogens become equatorial. Compare the motion along this normal mode with the idealized Berry pseudorotation motion shown in Figure 1. Providing additional support for the argument that this mode is indeed the one appropriate to a Berry pseudorotation pathway is the result obtained when an AM1 trajectory (DRC)[35] is computed starting in the direction of this mode with 5.0 kcal/mol of excess kinetic energy. The motion along the trajectory carries the molecule smoothly to the transition state for the Berry pseudorotation and then along to the equivalent isomer with H_1 and H_2 axial and the two axial hydrogens equatorial.

The normal-mode frequencies for the C_{4v} structure of SiH_5^- are given in Table VI. Again, we find general agreement among the various methods in these calculated frequencies. The decomposition of these normal-mode motions at the MP2/6-31G(d) level is given in Table VII. This analysis illustrates that the five highest frequency modes are Si–H stretches, with ν_1 containing a significant amount of the Si–H_{ap} stretch. Mode ν_6 (Table IV) has the required imaginary frequency that establishes the structure as the expected transition state; analysis of the atom motions (see also Table VII) confirms that this mode has the motion appropriate to a Berry pseudorotation transition state. The remaining normal modes are dominated by H–Si–H bending motions.

It is revealing to compare the calculated intrinsic frequencies with the trends in bond lengths (and implied bond strengths) noted above. The MP2/6-31G(d) frequencies for the Si–H stretches are 2111, 1960, 1730, and 1590 cm^{-1}, respectively, for the apical (C_{4v}), equatorial (D_{3h}), basal (C_{4v}), and axial (D_{3h}) hydrogens. This is in complete agreement with the trend noted earlier and lends credence to the implied bond strengths.

(35) Stewart, J. J. P.; Davis, L. P.; Burggraf, L. W. *J. Comput. Chem.* **1987**, *8*, 1117–1123.
(36) Miller, W. H.; Handy, N. C.; Adams, J. E. *J. Chem. Phys.* **1980**, *72*, 99.
(37) Pople, J. A.; Luke, B. T.; Frisch, M. J.; Binkley, J. S. *J. Phys. Chem.* **1985**, *89*, 2198.

Table IV. Harmonic Normal-Mode Frequencies (cm^{-1}) for D_{3h} Structure of SiH_5^-

	ν_1	ν_2	ν_3	ν_4	ν_5, ν_6	ν_7, ν_8	ν_9, ν_{10}	ν_{11}, ν_{12}
symmetry	A_1'	A_1'	A_2'	A_2''	E′	E′	E′	E″
MNDO	2206	1802	1938	1146	2067	1092	510	1227
AM1	2149	1834	1986	953	2113	884	540	1091
PM3	1889	1718	1810	807	1904	748	567	943
RHF/6-31G(d)	2082	1414	1590	1089	2031	1136	583	1305
RMP2/6-31G(d)	2014	1460	1608	1079	1986	1101	538	1257
RMP2/6-31++G(d,p)	2052	1438	1594	1032	2031	1070	557	1243

Table V. Percentage Contribution of Internal Coordinates to Normal-Mode Frequencies: Trigonal-Bipyramidal Structure[a]

	$Si-H_{ax}$	$Si-H_{eq}$	$H_{ax}-Si-H_{eq}$	$H_{eq}-Si-H_{eq}$
ν_1	0.20	0.80	0.00	0.00
ν_2	0.80	0.20	0.00	0.00
ν_3	0.97	0.00	0.03	0.00
ν_4	0.03	0.00	0.97	0.00
ν_5, ν_6	0.00	1.00	0.00	0.00
ν_7, ν_8	0.00	0.00	0.88	0.12
ν_9, ν_{10}	0.00	0.00	0.12	0.87
ν_{11}, ν_{12}	0.00	0.00	1.00	0.00

[a] H_{ax} = axial hydrogen, H_{eq} = equatorial hydrogen. The first two colums are stretching motions. The second two columns are bending motions.

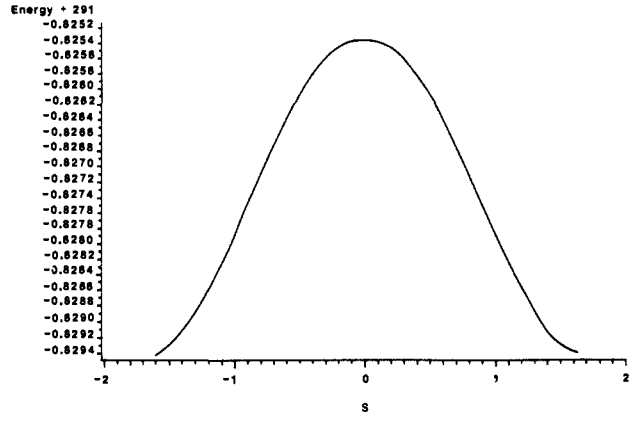

Figure 3. SiH_5^- MP2/6-31G(d) IRC (energy, hartrees; s, $amu^{1/2}$·bohr.

Intrinsic reaction coordinate calculations were run starting at each of the semiempirical and MP2/6-31G(d) saddle points. These IRC's confirm that these transition states do indeed connect two trigonal-bipyramidal D_{3h} structures, each with a different pair of hydrogen atoms axial. A plot of the MP2/6-31G(d) energy along the IRC is given in Figure 3.

It is instructive to plot the generalized MP2/6-31G(d) normal-mode frequencies as a function of the distance along the C_{2v} path corresponding to the IRC. Figure 4 illustrates the variation of the a_1 and a_2 generalized normal-mode frequencies along the IRC, while Figure 5 contains the analogous curves for the b_1 and b_2 modes. To aid reading these figures, the correlation among C_{4v}, C_{2v}, and D_{3h} irreducible respresentations is given in Table VIII. Furthermore, note that only $3N - 7$ modes are plotted, since the gradient (IRC) direction has been projected out to obtain proper normal modes.[36]

Vibrational analysis of the frequencies shown in Figures 4 and 5 reveals the detailed nature of these modes along the IRC. At the C_{4v} saddle point, the a_2 mode is an H_b-Si-H_b bend (b = basal). As the structure moves to the D_{3h} minimum, the contribution from one of the H_b-Si-H_a (a = apical) bends increases and the two a_2 contributions become equivalent $H_{eq}-Si-H_{eq}$ (eq = equatorial) bends. Similar comments apply to the other normal modes, with very little stretch–bend interaction throughout the IRC.

The variation of the intrinsic frequencies along the IRC is illustrated in Figure 6, with the internal coordinates described in Figure 7. At the saddle point, stretch 1 corresponds to an apical Si–H bond, while stretch 2 and stretch 3 are equivalent basal Si–H stretching motions. As the molecule moves down the IRC,

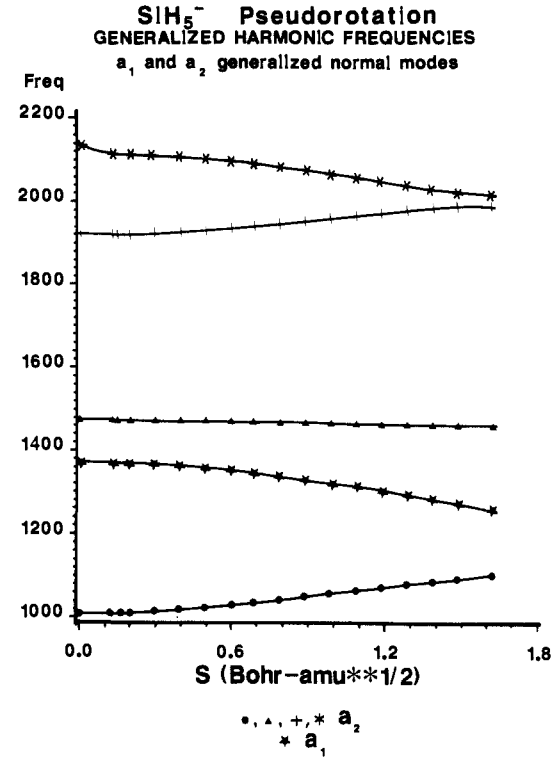

Figure 4. Plot of a_1 and a_2 generalized normal-mode frequencies (cm^{-1}) along the 6-31G(d) IRC.

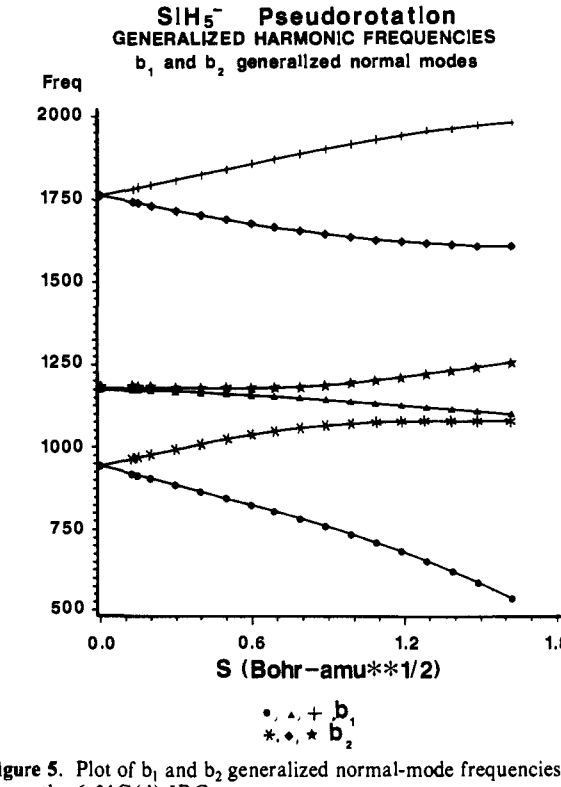

Figure 5. Plot of b_1 and b_2 generalized normal-mode frequencies (cm^{-1}) along the 6-31G(d) IRC.

Table VI. Harmonic Normal-Mode Frequencies (cm^{-1}) for C_{4v} Structure of SiH_5^-

	ν_1	ν_2	ν_3	ν_4	ν_5	ν_6	ν_7, ν_8	ν_9, ν_{10}	ν_{11}, ν_{12}
symmetry	A_1	A_1	A_1	B_1	B_2	B_2	E	E	E
MNDO	2218	2088	1073	1351	1785	389*i*	1981	1133	954
AM1	2219	2092	861	1204	1817	456*i*	2026	973	854
PM3	1987	1851	777	962	1712	541*i*	1836	855	740
RHF/6-31G(d)	2145	1956	1081	1425	1447	452*i*	1779	1222	1006
RMP2/6-31G(d)	2114	1920	1009	1371	1475	412*i*	1760	1174	942
RMP2/6-31++G(d,p)	2152	1951	1015	1356	1460	432*i*	1779	1143	957

Table VII. Percentage Contributions of Internal Coordinates to Normal-Mode Frequencies: Tetragonal Structure[a]

	Si–H_a	Si–H_b	H_a–Si–H_b	H_b–Si–H_b
ν_1	0.98	0.02	0.00	0.00
ν_2	0.02	0.98	0.00	0.00
ν_3	0.00	0.00	0.87	0.13
ν_4	0.00	0.00	0.00	1.00
ν_5	0.00	0.98	0.00	0.02
ν_6	0.00	0.02	0.98	0.00
ν_7, ν_8	0.00	0.98	0.00	0.00
ν_9, ν_{10}	0.00	0.02	0.00	0.98
ν_{11}, ν_{12}	0.00	0.00	1.00	0.00

[a] H_a = apical hydrogen; H_b = basal hydrogen.

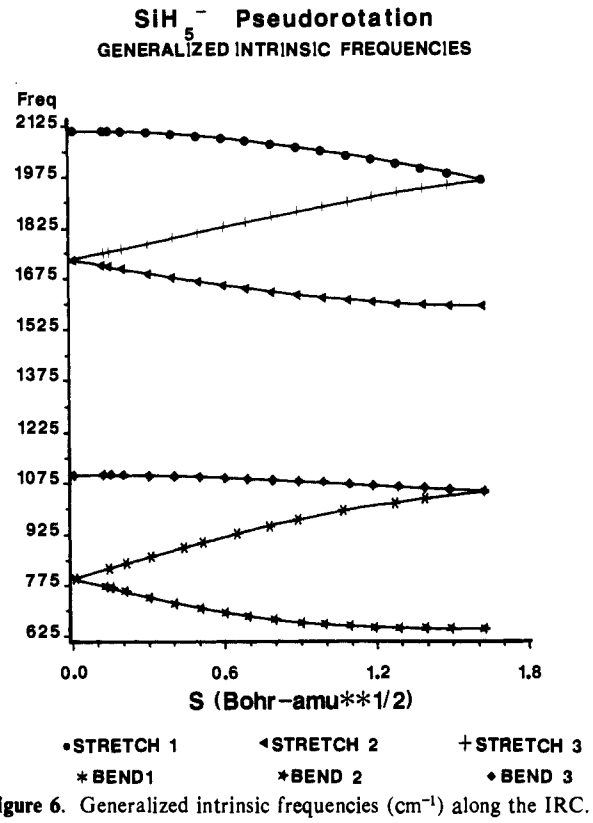

Figure 6. Generalized intrinsic frequencies (cm^{-1}) along the IRC.

stretches 1 and 3 become equivalent equatorial Si–H motions while stretch 2 transforms into one of the axial Si–H stretches. The bending motions evolve in a similar manner. At the transition state, bend 3 is an H_b–Si–H_b bend, while bend 1 and bend 2 are equivalent H_a–Si–H_b bending motions. Upon relaxation, bends 1 and 3 become equivalent H_{eq}–Si–H_{eq} bends while bend 2 transforms into the H_{ax}–Si–H_{ax} bend.

Table VIII. Correlation of Irreducible Representations

C_{4v}	C_{2v}	D_{3h}
A_1, B_2	A_1	A_1', E'
B_1	A_2	E''
E	B_1	E', A_2'
E	B_2	E', A_2''

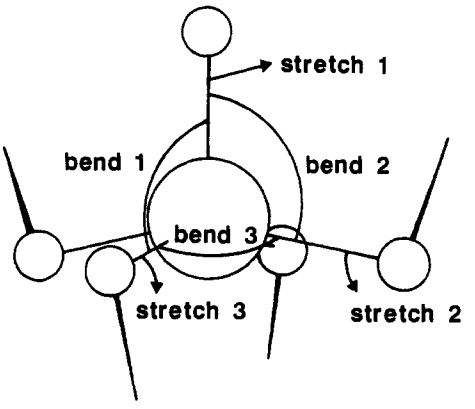

Figure 7. Schematic of internal coordinates for the pseudorotation motion.

This completes our analysis of SiH_5^-. We have shown general agreement among these sets of calculations and previous calculations for structures and energetics of this prototype silicon pentacoordinated molecule. We have established a low barrier to Berry pseudorotation and completed a normal-coordinate analysis of both structures that are stationary points on the potential surface. We have, for the first time, established (at this level of theory) that the C_{4v} square-pyramidal structure of SiH_5^- is the transition state for Berry pseudorotation of one D_{3h} trigonal-bipyramidal structure into an equivalent bipyramidal structure. In future papers of this series, we will turn our attention to generalization of pseudorotation of anionic silicon pentacoordinated structure by considering halogen-substituted anions and by examining the details of the dynamics of the pseudorotation process.

Acknowledgment. This work was supported in part by grants (to M.S.G.) from the Air Force Office of Scientific Research (87-0049), the National Science Foundation (CHE86-40071), and the Petroleum Research Fund, administered by the American Chemical Society. The calculations were performed on the quantum chemistry VAX 8530, purchased with the assistance of DoD Grant 86-0237. We are also grateful to Dr. Jerry Boatz for his assistance with the vibrational analysis.